# Role of Helix Nucleation in the Kinetics of Binding of Mastoparan X to Phospholipid Bilayers†

Jia Tang,‡ Rachel S. Signarvic,§ William F. DeGrado,‡,§ and Feng Gai*,‡

*Department of Chemistry and Department of Biochemistry and Biophysics, University of Pennsylvania, Philadelphia, Pennsylvania 19104*

*Received September 9, 2007; Revised Manuscript Received October 1, 2007*

ABSTRACT: Many antimicrobial peptides undergo a coil-to-helix transition upon binding to membranes. While this conformational transition is critical for function, little is known about the underlying mechanistic details. Here, we explore the membrane-mediated folding mechanism of an antimicrobial peptide, mastoparan X. Using stopped-flow fluorescence techniques in conjunction with a fluorescence resonance energy transfer (FRET) pair, *p*-cyanophenylalanine (donor) and tryptophan (acceptor), we were able to probe, albeit in an indirect manner, the membrane-mediated folding kinetics of this peptide. Our results show that the association of mastoparan X with model lipid vesicles proceeds with biphasic kinetics. The first step shows a large change in the FRET signal, indicating that the helix forms early in the time course of the interaction, while the second step where a further increase in tryptophan fluorescence is observed presumably reflects deeper insertion of the peptide into the bilayer. Additional kinetic studies on a double mutant of mastoparan X, designed to form a nucleation site for α-helix formation through coordination with a metal ion (e.g., $Zn^{2+}$ or $Ni^{2+}$), indicate that while the coil-to-helix transition occurs in the first step, it follows the rate-determining docking of the peptide onto the membrane surface. Taken together, these results indicate that the initial association of the peptide with the membrane occurs in a nonhelical conformation, which rapidly converts to a helical state within the anisotropic environment of the bilayer surface.

Peptide−membrane interactions play a crucial role in a wide range of biological processes, such as membrane lysis, viral fusion, and cellular signaling (*1*−*3*). Many membrane peptides, such as antimicrobial peptides (AMPs), are often unstructured in solution and thus require folding for function. For example, most linear AMPs adopt an α-helical structure when associated with membranes, and it has been shown that the hemolytic activity of an AMP is correlated with its helicity (*4*−*7*). While there have been a plethora of studies focusing on various structural and thermodynamic aspects of membrane peptides (*7*−*16*), there have been far fewer experiments that aimed to understand the kinetic and/or mechanistic details of the respective membrane-mediated folding process, largerly due to the lack of appropriate experimental methods and probes.

Thus, for many AMPs, when and where the α-helical conformation is formed and what determines the folding dynamics remain unclear. One model proposes that helix formation is concurrent with the process of binding and occurs at the interfacial region of lipid bilayers (*17*−*24*), followed by insertion, whereas a different view suggests that the coil-to-helix transition occurs only after the peptide is inserted (*25*, *26*). Recently, using magainin 2 as a model system, we have shown that it is possible to probe the membrane-mediated helix folding process of an AMP through the use of an amino acid FRET pair in conjunction with a stopped-flow technique (*23*). Our results suggest that the folding of this peptide is coupled to its initial binding to lipid vesicles and occurs at the interfacial region of the membrane. However, to substantiate this conclusion, further studies on different peptides are necessary.

In this paper, we explore the role of helix formation in the binding of the amphiphilic α-helical peptide mastoparan X (sequence, INWKGIAAMAKKLL) to lipid bilayers. Mastoparan X (termed MPx thereafter) is a peptidic toxin isolated from wasp venom which can disrupt cell membranes by forming transient pores (*7*, *27*−*30*). It has been shown by both NMR and circular dichroism (CD) spectroscopies that MPx is unstructured in aqueous solution but folds to an α-helical conformation when bound to lipid vesicles (*31*, *32*). Specifically, we use two approaches to probe the kinetics of helix formation and membrane association of this peptide. First, we use the aforementioned FRET assay which relies on the fact that the average end-to-end distance decreases appreciably when MPx undergoes a transition from a random coil ensemble in water to an α-helical conformation, either when it binds to membrane surfaces or when it is in the presence of the helix-promoting solvent 2,2,2-trifluoroethanol (TFE). For this purpose, we added a *p*-cyanophenylalanine ($Phe_{CN}$) residue to the C-terminus of MPx (the resultant peptide is named MPx-P15). $Phe_{CN}$ is a fluorescent amino

† Supported by the National Institutes of Health (Grants GM-065978 and RR-01348) and the National Science Foundation (Grant DMR05-20020).

* To whom correspondence should be addressed. Telephone: (215) 573-6256. Fax: (215) 573-2112. E-mail: gai@sas.upenn.edu.

‡ Department of Chemistry.

§ Department of Biochemistry and Biophysics.

10.1021/bi7018404 CCC: $37.00 
Published on Web 11/10/2007

acid that can undergo energy transfer to tryptophan (Trp) with an $R_0$ of ca. 16 Å (*33*, *34*). This distance is particularly convenient for this application as it is large enough to be sensitive to helix formation given the spacing of the Trp and $Phe_{CN}$ residues but small enough to minimize adventitious intermolecular FRET within the relatively crowded confines of a bilayer. If one directly excites Trp at 290 nm, where the absorbance of $Phe_{CN}$ is comparatively small, the kinetics of insertion of the Trp residue and thus the association of MPx with lipid bilayers can be monitored. However, the time course obtained by this method cannot discern helix formation. On the other hand, excitation of $Phe_{CN}$ at 240 nm leads to enhanced Trp fluorescence due to FRET if helix formation accompanies the insertion of the Trp residue into the bilayer. Via a comparison of the association kinetics with excitation at either 240 or 290 nm, it is therefore possible to assess the kinetic step in which the helix folding occurs. For example, in the case of a biphasic reaction, which is often observed for peptide−membrane association (*21*, *23*, *25*), one can compare the time courses obtained using these two excitation wavelengths to determine which step involves helix formation; if folding occurs in the first kinetic step, then the amplitude of this phase will be greater when Trp is excited at 240 nm compared to direct excitation at 290 nm, because helix formation enhances the Trp fluorescence due to the enhanced FRET.

Consistent with our earlier study (*23*), the current stopped-flow FRET results also suggest that MPx becomes folded once it adsorbs onto the model membrane surface. However, this FRET method cannot determine the role of helix formation in this reaction. To distinguish whether the helix forms before, after, or concomitant with the formation of the transition state (TS) ensemble of this initial binding phase, we use the second method in which a metal-binding site is introduced into MPx to form a folding nucleus for α-helix formation. Previous work has shown that histidine (His) residues separated by a single turn of an α-helix (i.e., a $HX_3H$ segment) bind $Zn^{2+}$ or $Ni^{2+}$ ions at micromolar metal ion concentrations, and that this interaction can stabilize the formation of monomeric helices (*35*, *36*). Also, stabilization of the α-helical conformation can indirectly stabilize the dimerization of α-helical coiled coils as well as the folding of globular helical proteins (*37*−*40*). To the extent that the α-helix is formed in the TS ensemble, the rate of dimerization of coiled coils or folding of globular proteins is also increased (*41*−*43*). In a similar manner, it is possible to increase the affinity of amphiphilic peptides for membranes through the incorporation of helix-stabilizing metal ion-binding sites. Previously, we have incorporated His residues at positions 4 and 8 of MPx, leading to a peptide (named MxHH) whose hemolytic potency and affinity for phospholipid bilayers are increased in the presence of metal ions (*44*). Here, we further use MxHH (sequence, INW**H**GIA**H**MAKKLL) to examine the effect of nucleation on the membrane-mediated α-helix folding kinetics. To this end, if the α-helix is formed in the transition state of the initial binding step, then one observes an increase in the rate of this step due to stabilization of the α-helical conformation through coordination of a metal ion (e.g., $Zn^{2+}$ or $Ni^{2+}$) with the histidine ligands, whereas a small effect is observed if helix formation occurs subsequent to formation of the respective transition state.

## MATERIALS AND METHODS

*Materials.* All peptides used in the current study were synthesized using the standard Fmoc-based solid-phase method, purified by reverse-phase high-performance liquid chromatography, and verified by mass spectrometry. Respective peptide stock solutions were first adjusted to neutral pH with 1.0 M NaOH and then diluted with either 10 mM Tris buffer (pH 7.0) for CD measurements or 25 mM HEPES buffer (pH 7.0) for fluorescence experiments. The final peptide concentration of each sample was determined optically using the absorbance at 280 nm and $\epsilon_{280}$ values of 6440 and 5600 $M^{-1}$ $cm^{-1}$ for MPx-P15 and MxHH, respectively. 1-Palmitoyl-2-oleoyl-*sn*-glycero-3-phosphocholine (POPC) was purchased from Avanti Polar Lipids (Alabaster, AL). All $Zn^{2+}$ and $Ni^{2+}$ solutions were freshly prepared from reagent-grade $ZnCl_2$ and $NiSO_4 \cdot 6H_2O$ (Sigma, St. Louis, MO), respectively, before each experiment.

*Vesicle Preparation.* POPC solutions (2 mM) were first prepared in 25 mM HEPES buffer (pH 7.0) or 10 mM Tris buffer (pH 7.0) and then taken through a freeze−thaw−vortex process. After this cycle was repeated five times, the vesicle suspension was extruded through a polycarbonate membrane filter with pore diameters of 200 or 50 nm (for SPR measurement) using an extruder (Avanti Polar Lipids, Alabaster, AL). Vesicle solutions used in CD experiments were further sonicated in an ultrasonic bath (Branson Ultrasonics) until they were clear.

*CD Measurement.* The far-UV CD spectra at 20 °C were collected on an AVIV 62DS spectropolarimeter (Aviv Associates, Edison, NJ) using a 1 cm quartz cell. The peptide and POPC vesicle concentrations were 10 $\mu$M and 1 mM, respectively. Mean residue ellipticity was calculated using the equation $[\theta] = (\theta_{obs}/10lc)/N$, where $\theta_{obs}$ is the ellipticity in millidegrees, $l$ is the optical path length (centimeters), $c$ is the concentration of the peptide (molar), and $N$ is the number of residues.

*Absorption Measurement.* All UV−vis spectra were measured on a Lambda 25 UV−vis spectrometer (Perkin-Elmer).

*Surface Plasmon Resonance (SPR) Measurement.* SPR measurement of binding of MPx-P15 to a POPC hybrid bilayer membrane was carried out using an FT-SPR 100 apparatus (Thermo Fisher Scientific, Inc.). The details of the experiment are described in the Supporting Information.

*Fluorescence Measurement.* The fluorescence spectra were collected on a Fluorolog 3.10 spectrofluorometer (Jobin Yvon Horiba) using a 1 cm quartz sample holder. The spectral resolution was 2 nm (for both excitation and emission). The temperature was maintained at 20 °C using a TLC 50 Peltier temperature controller (Quantum Northwest). The peptide and vesicle concentrations were 2 $\mu$M and 1 mM, respectively.

*Stopped-Flow Fluorescence Measurements.* The stopped-flow fluorescence kinetics were measured using a SFM-300 stopped-flow module (Bio-logic, Claix, France) equipped with home-built optics, the details of which have been described elsewhere (*23*). In this study, a microcuvette ($\mu$FC-08) with an optical path length of 0.8 mm was used, which gave rise to a dead time of ~800 $\mu$s. The peptide−vesicle association reactions were initiated by mixing equal volumes of corresponding peptide and vesicle solutions. For experiments in which $Zn^{2+}$ or $Ni^{2+}$ was involved, either the peptide

or vesicle solution contains the desired metal ion (i.e., $ZnCl_2$ or $NiSO_4$). The final concentrations of the peptide, POPC, and metal ion were 4 $\mu$M, 1 mM, and 300 $\mu$M, respectively. All stopped-flow experiments were carried out at 20 °C. A long-pass filter with a cut-on wavelength of 315 nm (Edmund Industrial Optics) was used to eliminate the excitation light and also the $Phe_{CN}$ fluorescence (for MPx-P15). All reported errors were obtained from the standard deviation of repeated measurements.

## RESULTS

*Static CD Measurements*. Similar to many antimicrobial peptides, MPx has been shown to undergo a coil-to-helix transition upon binding to lipid vesicles (*31*, *32*). Consistent with this picture, the far-UV CD spectra of MPx-P15 (Figure S1, Supporting Information) show that it is essentially unfolded in buffer solution but folds into an α-helical conformation when bound to POPC vesicles (binding of MPx-P15 to POPC membranes was verified by SPR spectroscopy; see Figure S2 of the Supporting Information for details). This indicates that adding a $Phe_{CN}$ residue to the C-terminus of MPx does not change, in any significant manner, its membrane binding properties. To examine the effect of metal binding, we also measured the CD spectra of MxHH in the presence and absence of metal ions and POPC vesicles (Figure S3, Supporting Information). In the absence of vesicles, the addition of $Zn^{2+}$ has no significant effect on the CD spectrum of MxHH, and the addition of $Ni^{2+}$ gives rise to a small increase in the ellipticity near 222 nm. On the other hand, MxHH forms a helical conformation in the presence of saturating concentrations of lipids, with or without the presence of metal ions. Thus, these results are entirely consistent with the study of Ghadiri et al. (*35*) showing that the addition of metal ions to $HX_3H$ peptides can bias the monomeric structure toward a helical conformation but not tip the balance toward a fully helical structure in the absence of other stabilizing features. On the other hand, the metal-binding $HX_3H$ motif can lend additional metal ion-dependent stability to fully formed helices (*40*−*42*). Our earlier work has also shown that these metal ion concentrations lead to a 5−10-fold increase in the affinity of MxHH for POPC bilayers and hemolytic potency (*44*).

*Static Fluorescence Measurement*. The native Trp residue in MPx and MPx-P15 is a convenient fluorescent probe of peptide−membrane association (*27*−*29*) due to the sensitivity of Trp fluorescence to environments. As expected (Figure 1a), binding of MPx-P15 to POPC vesicles results in a significant change in the Trp fluorescence spectrum when the indole fluorophore is directly (and selectively) excited at 290 nm. Compared to that obtained in buffer solution, the fluorescence spectrum of MPx-P15 obtained in POPC vesicle solutions is more intense and also shifted to a lower wavelength, indicating that in the membrane-bound state the Trp side chain samples a more hydrophobic and/or rigid environment.

On the other hand, when excited at 240 nm, where the absorption cross section of $Phe_{CN}$ overwhelms that of Trp (*34*), the emission spectra of MPx-P15 in both buffer and POPC vesicle solutions show characteristics of FRET (Figure 1b), indicating that in both cases the separation distance between $Phe_{CN}$ and Trp is well within $2R_0$ (ca. 32 Å).

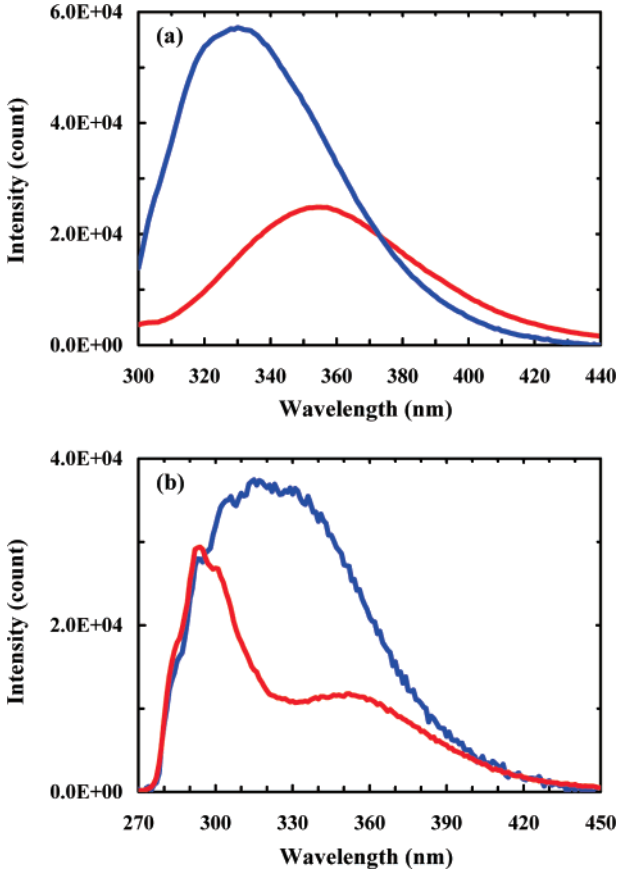


FIGURE 1: Fluorescence spectra of MPx-P15 in 25 mM HEPES buffer at pH 7 (red) and 1 mM POPC vesicle (blue) solutions: (a) $\lambda_{ex}$ = 290 nm and (b) $\lambda_{ex}$ = 240 nm.

Nevertheless, in the case of POPC vesicles, the donor emission is further reduced with the concomitant increase in the acceptor fluorescence. This result, consistent with the static CD measurements, indicates that MPx-P15 folds into an α-helix from a nonhelical conformation upon binding to membranes, a conformational transition that will shorten the distance between $Phe_{CN}$ and Trp and further lead to an enhanced FRET efficiency. The fluorescence spectrum of MPx-P15 in 20% TFE solution, where MPx-P15 also adopts an α-helical structure, further corroborates this observation (Figure S4, Supporting Information). Taken together, these results indicate that the α-helix folding process of MPx-P15 upon association with POPC vesicles can be identified by comparing the stopped-flow Trp fluorescence traces obtained with direct (i.e., $\lambda_{ex}$ = 290 nm) and indirect (i.e., via FRET using $\lambda_{ex}$ = 240 nm) excitations of the indole fluorophore (*23*).

We have also measured the Trp fluorescence spectra of MxHH under different conditions, i.e., in buffer and POPC vesicle solutions, as well as with and without $Ni^{2+}$ and $Zn^{2+}$ ions (data not shown). Similar to that observed for MPx-P15, membrane association induces an increase in the intensity and also a blue shift of the Trp fluorescence spectrum of MxHH; however, as observed in other studies (*45*, *46*), $Ni^{2+}$ was found to substantially quench the Trp fluorescence (by ca. 30%).

*Stopped-Flow Kinetics of MPx-P15*. The kinetics of peptide−vesicle association of MPx-P15 were investigated by a stopped-flow fluorescence technique (*23*). First, the Trp was directly (and selectively) excited at 290 nm. As shown

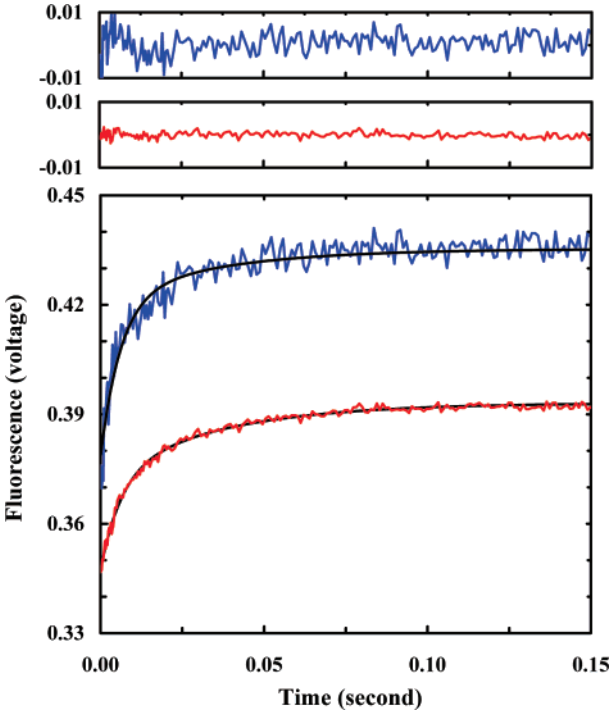


FIGURE 2: Representative stopped-flow fluorescence traces obtained with a 315 nm long-pass filter. The excitation wavelengths were 290 (red) and 240 nm (blue). The corresponding reactions were initiated by mixing an 8 $\mu$M MPx-P15 solution with a 2 mM POPC vesicle solution at 20 °C. Smooth lines are global fits to the equation $F(t) = A - B_1 \times \exp(-k_1 t) - B_2 \times \exp(-k_2 t)$, where $k_1 = 163$ s$^{-1}$ and $k_2 = 28$ s$^{-1}$. When $\lambda_{ex} = 240$ nm, $A = 0.435$, $B_1 = 0.043$, and $B_2 = 0.014$; when $\lambda_{ex} = 290$ nm, $A = 0.393$, $B_1 = 0.025$, and $B_2 = 0.021$. The data obtained at 290 nm have been scaled and offset for easy comparison. The residuals of these fits are shown in the top panels [290 (red) and 240 nm (blue)].

(Figure 2), rapid mixing of MPx-P15 with POPC vesicles results in an increase in the Trp fluorescence, consistent with the equilibrium results. In addition, the resultant stopped-flow kinetics can be fit by a double-exponential function with two well-separated rate constants, i.e., 163 ± 27 and 28 ± 4 s$^{-1}$, respectively, suggesting that the peptide−membrane association proceeds through a kinetic intermediate. Similar biphasic kinetics have also been observed for other membrane binding peptides (*21*, *25*, *47*). For example, a stopped-flow Trp fluorescence study shows that the association of melittin, a structural analogue of MPx, with zwitterionic membranes also occurs over a double-exponential time course on the millisecond time scale (*21*). Furthermore, these kinetic events have been attributed to the initial adsorption of the melittin at the lipid−water interface and a subsequent deeper insertion of the peptide into the membrane interior. In view of these previous studies, we assign the first or faster phase of the stopped-flow kinetics to the initial binding of MPx-P15 to the vesicle surface and the second one to an insertion process that further incorporates the surface-bound peptide into a more deeply buried position inside the membrane. Previous equilibrium studies conducted under similar experimental conditions have shown that the membrane-bound MPx α-helix rests at a slightly oblique angle nearly parallel to the membrane surface (*11*, *48*).

While the aforementioned stopped-flow kinetics describe the time course during which the peptide molecules are incorporated into the POPC vesicles, these data alone do not provide a structural interpretation of the respective kinetic steps. Therefore, we have carried out further stopped-flow experiments in which the Trp fluorescence was induced via indirect excitation of the indole chromophore, i.e., via the mechanism of FRET. As shown (Figure 2), the stopped-flow Trp fluorescence kinetics obtained with an excitation wavelength of 240 nm, where the absorption cross section of $Phe_{CN}$ overwhelms that of Trp, also consist of two distinguishable kinetic phases. A quantitative analysis involving the global fitting of the kinetic traces obtained with both excitation wavelengths (i.e., 240 and 290 nm) indicates that these data can be fit adequately by two double-exponential functions that differ only in their relative amplitudes. In particular, changing the excitation wavelength from 290 to 240 nm results in an increase in the relative amplitude of the faster phase, i.e., from 55 ± 6 to 75 ± 8%, suggesting that this kinetic step reports not only the initial peptide−vesicle binding event, which leads to the initial burial of the indole ring in a more hydrophobic environment, but also the corresponding α-helix folding process. As discussed above, the formation of an α-helical structure upon membrane association brings the donor and acceptor closer, thus leading to an increase in the relative amplitude of the kinetic phase reporting this event when the Trp fluorescence is excited via FRET assuming that the fluorescence quantum yield of the donor does not change significantly upon peptide−membrane association. However, it is worth noting that while this result suggests that macroscopically the α-helix forms concomitantly with the initial binding, at the molecular level folding could occur either immediately prior to or after this process. To address this issue, we investigated the MxHH peptide, the helical nucleation of which could be modulated by addition of metal ions.

*Stopped-Flow Kinetics of MxHH.* The initial rate of binding of MPx-P15 (i.e., $k_1$) to the POPC vesicle is slower than the pertinent diffusion-limited rate estimated for peptides of similar size (*49*, *50*), suggesting that a conformational change is required before the peptide can be adsorbed onto the vesicle surface. In light of the above suggestion that the α-helical structure is formed concomitantly with the initial binding process, a possible scenario would be that such adsorption requires the peptide to be prefolded into an α-helical structure. To test this possibility, we have further studied the kinetics of peptide−vesicle association of MxHH in the presence and absence of metal ions ($Ni^{2+}$ or $Zn^{2+}$). If a preformed α-helix is indeed a prerequisite for binding, one would expect that coordination with a metal ligand will enhance the initial rate of binding of MxHH to POPC vesicles because the metal-bound MxHH is designed to form an α-helical folding nucleus that can accelerate the folding of helical peptides and proteins (*41*, *42*, *51*). As indicated (Figure 3), our results show that the presence of $Ni^{2+}$ or $Zn^{2+}$ does not change (within our experimental uncertainties) the initial rate of binding (i.e., $k_1$) of MxHH to POPC vesicles. The rate constants of the first phase in the respective stopped-flow kinetics are determined to be 168 ± 16, 176 ± 14, and 163 ± 12 s$^{-1}$ for MxHH, $Zn^{2+}$-bound MxHH, and $Ni^{2+}$-bound MxHH, respectively, which is suggestive of a scenario in which the helix is formed only after the peptide is bound to the membrane surface. Interestingly, at relatively longer time scales, the stopped-flow kinetics of $Ni^{2+}$-bound MxHH are distinctly different from those of $Zn^{2+}$-bound MxHH, most noticeably with a more pronounced second phase and

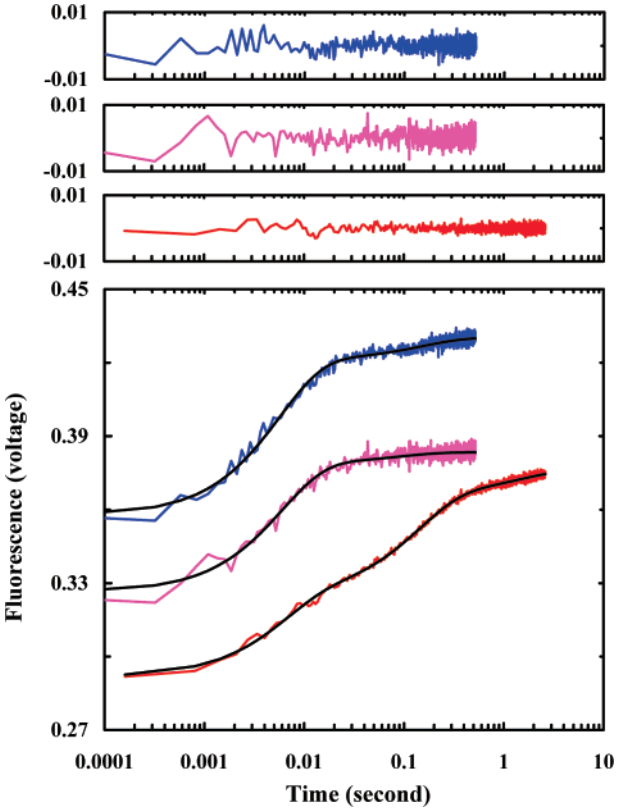


FIGURE 3: Representative stopped-flow fluorescence traces obtained by mixing an 8 $\mu$M peptide solution, i.e., MxHH (pink), $Zn^{2+}$-bound MxHH (blue), or $Ni^{2+}$-bound MxHH (red), with a 2 mM POPC vesicle solution at 20 °C. The smooth lines are fits to the equation $F(t) = A - B_1 \times \exp(-k_1 t) - B_2 \times \exp(-k_2 t) - B_3 \times \exp(-k_3 t)$. For MxHH, $k_1 = 168\ s^{-1}$, $k_2 = 12\ s^{-1}$, $A = 0.383$, $B_1 = 0.052$, $B_2 = 0.005$, and $B_3 = 0$. For $Zn^{2+}$-bound MxHH, $k_1 = 176\ s^{-1}$, $k_2 = 6\ s^{-1}$, $A = 0.430$, $B_1 = 0.063$, $B_2 = 0.010$, and $B_3 = 0$. For $Ni^{2+}$-bound MxHH, $k_1 = 163\ s^{-1}$, $k_2 = 7\ s^{-1}$, $k_3 = 0.7\ s^{-1}$, $A = 0.376$, $B_1 = 0.033$, $B_2 = 0.041$, and $B_3 = 0.011$. These data have been offset for easy comparison. Top panels show the corresponding residuals of these fits.

an additional third phase with a rate constant of $0.7 \pm 0.2\ s^{-1}$ (Figure 3).

Because the presence of the metal ion could complicate kinetics in the monomeric state due to partial binding and changes in the unfolded state, we did not attempt to use the FRET method described above to probe the membrane-induced folding events of MxHH.

## DISCUSSION

Several models that aimed to describe the molecular mechanism of peptide−membrane interactions have been proposed. In particular, the Shai−Matsuzaki−Huang (SMH) model suggests that the peptide−membrane association follows a two-state model (*1*, *9*, *30*, *52*) in which the peptides, which are unfolded in the aqueous phase, first bind to the lipid−water interface and form an α-helical structure. This initial event is followed by the displacement of lipid molecules, the alteration of membrane structure, and in certain cases the entry of the peptide into the interior of the target cell (*1*). While this model is widely recognized, there have been only a few kinetic studies and simulations in which the nature of the respective conformational transitions has been investigated (*17*−*26*).

Previously, we have studied the membrane-mediated folding mechanism of magainin 2 using the FRET method described above (*23*). While our results are consistent with a picture in which folding precedes insertion (*22*), we were unable to determine whether the peptide adopts a full or partial helical conformation at the membrane surface due to the longer chain length of magainin 2 as well as whether folding is a prerequisite for binding. In an attempt to improve our understanding of the mechanism of such a membrane-mediated helical folding process, herein we studied a shorter antimicrobial peptide, MPx. In this case, the locations of the donor ($Phe_{CN}$) and acceptor (Trp) almost span the full length of the peptide; thus, the FRET signal should report the conformational change of the entire chain, rather than the local α-helix formation.

The equilibrium CD (Figure S1, Supporting Information) and fluorescence spectra (Figure 1) of MPx-P15 are consistent with other studies (*31*, *32*), showing that when mixed with POPC vesicles the peptide undergoes a coil-to-helix transition, and that in the vesicle-associated state the Trp side chain is sampling a more hydrophobic environment. Therefore, the Trp fluorescence was used to monitor the kinetics of peptide−vesicle association. Similar to those observed for other membrane-binding peptides and/or proteins (*21*, *23*, *25*, *47*), the stopped-flow Trp fluorescence kinetics triggered by mixing an 8 $\mu$M MPx-P15 solution with a 2 mM POPC vesicle solution, regardless of what excitation wavelength was used, show that the peptide−vesicle association proceeds in a biphasic manner on the millisecond time scale (Figure 2). On the basis of conclusions reached from similar studies (*21*, *23*, *25*) and the fact that the rate constant of the faster kinetic phase is linearly dependent on the concentration of vesicles used (data not shown), we assign this phase to an initial binding process in which the peptide is adsorbed onto the surface of the POPC vesicles to form a surface-bound state, and the slower one to a subsequent reorientation−insertion process during which the peptide becomes further integrated into the membrane to reach a membrane-bound state. In principle, the membrane-bound peptides can further aggregate to form pores or translocate across the membrane. However, under the current experimental conditions where the peptide-to-lipid ratio is very low ($\sim 4 \times 10^{-3}$), these processes are less likely to occur (*27*). In addition, such processes usually take place on the order of minutes, a time scale outside the current observation window (*27*−*29*).

More importantly, our stopped-flow kinetics obtained with different excitation wavelengths indicate that they differ only in the relative amplitudes of the respective steps. In particular, we find that the relative amplitude of the faster phase increases from ca. 55 to 75% when the excitation wavelength is changed from 290 to 240 nm, where the Trp fluorescence is excited via the mechanism of FRET. Since the FRET efficiency depends strongly on the distance between the donor and acceptor, this increase in amplitude thus likely indicates that the respective α-helical conformation of MPx-P15 (and MPx) is formed during this kinetic step. While the current FRET method does not directly report the secondary structural content of the peptide, our result is nevertheless consistent with several earlier studies (*17*−*24*). For example, using static infrared spectroscopy and a Langmuir trough technique, Silvestro and Axelsen (*19*) demonstrated that

cecropin A, a 37-residue antimicrobial polypeptide, adopts an α-helical structure while superficially adsorbed on the membrane surface. Using stopped-flow fluorescence and CD spectroscopies, Wang et al. (*17*). further showed that the respective helical structure of cecropin B forms early during its interaction with phospholipid vesicles and is populated as a kinetic intermediate prior to an insertion step that further integrates the peptide into the hydrophobic region of the membrane. In addition, several recent molecular dynamics simulations suggested a similar view. For example, the simulations of Im and Brooks (*22*) on a series of synthetic membrane peptides indicate that these peptides first become localized at the membrane−solvent interface where a significant amount of helical structures is formed and the complete insertion of the peptide into the membrane interior requires >80% helical content. Similarly, the coarse-grained molecular dynamics simulations of Bond and Sansom (*24*) on glycophorin also support the notion that the α-helix forms at the interfacial region of the membrane.

While the aforementioned FRET study is helpful in elucidating the nature of the conformational transition associated with the initial binding of MPx-P15 to POPC vesicles, it cannot distinguish whether folding occurs prior to binding or whether the α-helix is formed rapidly after the binding in response to the lower dielectric and highly anisotropic environment of the bilayer surface. In an attempt to distinguish these possibilities, we have studied the kinetics of membrane association of MxHH which was designed to form a helix nucleation site through metal binding, a strategy widely used to induce α-helix formation in peptides or proteins (*35*, *41*, *51*). Interestingly, our results show that, while the presence of metal ions strongly stabilizes the overall association of the helical peptide to the membrane, the initial rates of binding (i.e., $k_1$) of $Zn^{2+}$- and $Ni^{2+}$-bound MxHHs to POPC vesicles are (within experimental uncertainties) the same as that of MxHH (Figure 3). These results suggest that the α-helix structure is formed rapidly after the initial binding event (relative to the second phase of the reaction), in a process akin to a folding event occurring at the downhill side of a major folding free energy barrier (*53*, *54*). This observation is further corroborated by the fact that the initial binding rate of MPx-15 is almost identical to that of MxHH (i.e., 163 ± 27 and 168 ± 16 $s^{-1}$, respectively), although MPx-P15 has a larger mean helical propensity. Thus, our results not only are consistent with the notion that peptide−membrane interactions follow a sequential, multistage mechanism wherein the secondary structure is quickly formed at or near the membrane surface (*17*−*19*, *22*) but also provide new insights into the key conformational transitions. In summary, our results support the following mechanism of peptide−membrane association:

$$P_U + M \underset{k_{-S}}{\overset{k_S}{\rightleftharpoons}} [(P_UM)_S \underset{k_{-H}}{\overset{k_H}{\rightleftharpoons}} (P_HM)_S] \underset{k_{-I}}{\overset{k_I}{\rightleftharpoons}} (P_HM)_I$$

where $P_U$ and $P_H$ represent the unfolded and folded (i.e., helical) conformations of the peptide, respectively, and M stands for the model membrane. According to this scheme, $P_U$ and M first come together to form a surface-bound complex, $(P_UM)_S$. The actual second-order rate constant for this intermolecular reaction depends on the size of the peptide-binding site on the POPC vesicles. Once bound, the unfolded conformation can rapidly isomerize to form an α-helix, $P_H$, whose stability is enhanced on the membrane surface relative to that in aqueous solution. This first-order conformational process should occur with a relaxation time similar to that of helix formation, which occurs on the 100−500 ns time scale (*55*, *56*). Once the α-helix is formed, it can be further stabilized through formation of a more deeply inserted state $(P_HM)_I$, which occurs on a time scale slower than that of initial binding and helix formation. Depending on experimental conditions, the membrane-bound peptides can further interact to form oligmers or aggregates. Rigorously, the apparent rate constants obtained from the stopped-flow experiments (i.e., $k_1$ and $k_2$) are functions of the microscopic rate constants involved in the kinetic scheme described above. However, the fact that the stopped-flow fluorescence kinetics can be well fit by a double-exponential function with two well-separated rate constants indicates that $k_1$ is approximately equal to $k_S$.

The finding that the peptide can first bind to the membrane surface in a nonhelical state is consistent with earlier proposals (*5*, *49*, *57*) and also with the findings of the groups of Gellman and Shai, who have found that membrane binding and disruption need not involve a perfectly amphiphilic helical structure (*57*, *58*). Also, a large class of host defense peptides engages membranes in nonhelical conformations (*7*, *49*). Indeed, even short random polyacrylate copolymers with an appropriate balance of positively charged and hydrophobic groups display properties similar to those of antimicrobial peptides and helical peptide toxins (*59*, *60*). Thus, a peptide with both hydrophobic and charged groups would appear to be able to adopt a large number of conformations that position the apolar groups appropriately to bind to membrane surfaces. In the case of the peptides studied here, α-helix formation further stabilizes the overall complex but is not essential for its initial formation.

Both $Ni^{2+}$ and $Zn^{2+}$ were used to induce α-helix formation in MxHH; however, their effects on the stopped-flow kinetics of MxHH are different in one regard (Figure 3). While the stopped-flow kinetics of $Zn^{2+}$-bound MxHH are comparable to those of MxHH, which can be fit by a double-exponential function that is dominated by the faster component (~90% of the total signal), the stopped-flow kinetics of $Ni^{2+}$-bound MxHH show an additional slow phase. The stopped-flow fluorescence signals arising from the first two kinetic phases of $Ni^{2+}$-bound MxHH are almost identical to the total fluorescence signal obtained for $Zn^{2+}$-bound MxHH or MxHH. The additional slow phase observed in the presence of $Ni^{2+}$ is not relevant to the current investigation of the initial events in membrane association but could provide additional information concerning the mechanisms of insertion. This slow phase might be associated with a number of effects, including differential quenching of intermediate states, the kinetics of association and dissociation of ions from the peptide, or interactions of the metal ions with phospholipid molecules (*61*, *62*). To address the latter issue, we have also carried out stopped-flow experiments on MPx-P15 in the presence of $Zn^{2+}$ or $Ni^{2+}$. As shown (Figure 4), the stopped-flow kinetics triggered by mixing a peptide solution containing the corresponding metal ions with a POPC vesicle solution are almost identical (within experimental uncertainties) to that obtained without metal ions. For example, the rate constants of the first kinetic phase are

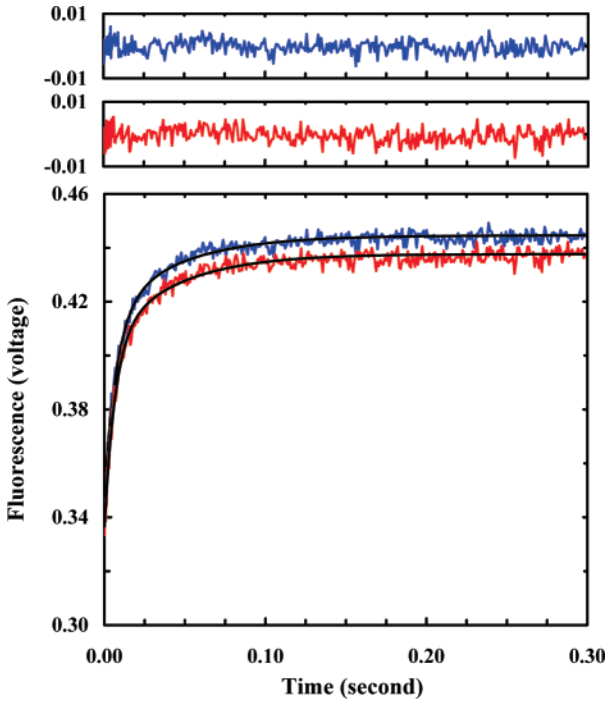


FIGURE 4: Stopped-flow kinetics obtained by mixing an 8 $\mu$M MPx-P15 peptide solution with a 2 mM POPC vesicle solution in the presence of $Zn^{2+}$ (blue) and $Ni^{2+}$ (red) at 20 °C. The smooth lines are fits to the double-exponential function $F(t) = A - B_1 \times \exp(-k_1 t) - B_2 \times \exp(-k_2 t)$. For MPx-P15 with $Ni^{2+}$, $k_1 = 152\ s^{-1}$, $k_2 = 24\ s^{-1}$, $A = 0.438$, $B_1 = 0.069$, and $B_2 = 0.033$, and for MPx-P15 with $Zn^{2+}$, $k_1 = 132\ s^{-1}$, $k_2 = 23\ s^{-1}$, $A = 0.445$, $B_1 = 0.067$, and $B_2 = 0.030$. The residuals of these fits are shown in the top panels.

determined to be 132 ± 18 and 152 ± 12 $s^{-1}$ for MPx-P15 mixed with $Zn^{2+}$ and $Ni^{2+}$, respectively, which are comparable to that determined for MPx-P15. These results, acting as control experiments, further support our observation that the incorporation of a metal-induced nucleation site does not accelerate the peptide−membrane binding kinetics. Therefore, the role of α-helix folding is primarily to stabilize the nascent surface-bound state of the peptide, rather than the initial binding event.

## CONCLUSION

In summary, we have employed an amino acid FRET pair, *p*-cyanophenylalanine and tryptophan, in conjunction with a stopped-flow fluorescence method to study the membrane-mediated folding kinetics of an antimicrobial peptide, mastoparan X. Our results show that the kinetics of peptide association with POPC vesicles occur over a double-exponential time course on the millisecond time scale and that the coil-to-helix transition takes place prior to the second kinetic phase. This result is consistent with our earlier study on magainin 2 and also several simulation studies. Furthermore, investigations of the vesicle association kinetics of MxHH, which is a double mutant of mastoparan X and designed to form a nucleation site for α-helix formation through coordination with a metal ion (e.g., $Zn^{2+}$ or $Ni^{2+}$), indicate that the formation of the corresponding α-helical conformation does not impose a large free energy barrier for peptide−membrane binding. Instead, its role is to stabilize the nascent surface-bound state.

## ACKNOWLEDGMENT

We also thank M. J. Tucker for synthesizing the peptide MPx-P15.

## SUPPORTING INFORMATION AVAILABLE

CD spectra of MPx-P15 and MxHH under different conditions, fluorescence spectra of MPx-P15 in buffer and 20% TFE solutions, and SPR measurements. This material is available free of charge via the Internet at http://pubs.acs.org.

## REFERENCES

1. Zasloff, M. (2002) Antimicrobial peptides of multicellular organisms, *Nature 415*, 389−395.
2. Mozsolits, H., Thomas, W. G., and Aguilar, M. I. (2003) Surface plasmon resonance spectroscopy in the study of membrane-mediated cell signaling, *J. Pept. Sci. 9*, 77−89.
3. Epand, R. M. (2003) Fusion peptides and the mechanism of viral fusion, *Biochim. Biophys. Acta 1614*, 116−121.
4. Dathe, M., Schümann, M., Wieprecht, T., Winkler, A., Beyermann, M., Krause, E., Matsuzaki, K., Murase, O., and Bienert, M. (1996) Peptide helicity and membrane surface charge modulate the balance of electrostatic and hydrophobic interactions with lipid bilayers and biological membranes, *Biochemistry 35*, 12612−12622.
5. Oren, Z., and Shai, Y. (1997) Selective lysis of bacteria but not mammalian cells by diastereomers of melittin: Structure−function study, *Biochemistry 36*, 1826−1835.
6. Chen, Y. X., Mant, C. T., Farmer, S. W., Hancock, R. E. W., Vasil, M. L., and Hodges, R. S. (2005) Rational design of α-helical antimicrobial peptides with enhanced activities and specificity/therapeutic index, *J. Biol. Chem. 280*, 12316−12329.
7. Toke, O. (2005) Antimicrobial peptides: New candidates in the fight against bacterial interactions, *Biopolymers 80*, 717−735.
8. Matsuzaki, K., Nakamura, A., Murase, O., Sugishita, K., Fuji, N., and Miyajima, K. (1997) Modulation of magainin 2-lipid bilayer interactions by peptide charge, *Biochemistry 36*, 2104−2111.
9. Huang, H. W. (2000) Action of antimicrobial peptides: Two-state model, *Biochemistry 39*, 8347−8352.
10. Dathe, M., Nikolenko, H., Meyer, J., Beyermann, M., and Bienert, M. (2001) Optimization of the antimicrobial activity of magainin peptides by modification of charge, *FEBS Lett. 501*, 146−150.
11. Tucker, M. J., Getahun, Z., Nanda, V., DeGrado, W. F., and Gai, F. (2004) A new method for determining the local environment and orientation of individual side chains of membrane-binding peptides, *J. Am. Chem. Soc. 126*, 5078−5079.
12. Ladokhin, A. S., and White, S. H. (2004) Interfacial folding and membrane insertion of a designed helical peptide, *Biochemistry 43*, 5782−5791.
13. Epand, R. M., Epand, R. F., Sayer, B. G., Melacini, G., Palgulachari, M. N., Segrest, J. P., and Anantharamaiah, G. M. (2004) An apolipoprotein AI mimetic peptide: Membrane interactions and the role of cholesterol, *Biochemistry 43*, 5073−5083.
14. Lopez, C. F., Nielsen, S. O., Moore, P. B., and Klein, M. L. (2004) Understanding nature's design for a nanosyringe, *Proc. Natl. Acad. Sci. U.S.A. 101*, 4431−4434.
15. Ringstad, L., Kacprzyk, L., Schmidtchen, A., and Malmsten, M. (2007) Effects of topology, length, and charge on the activity of a kininogen-derived peptide on lipid membranes and bacteria, *Biochim. Biophys. Acta 1768*, 715−727.
16. Thuduppathy, G. R., Craig, J. W., Kholodenko, V., Schon, A., and Hill, R. B. (2006) Evidence that membrane insertion of the cytosolic domain of Bcl-$X_L$ is governed by an electrostatic mechanism, *J. Mol. Biol. 359*, 1045−1058.
17. Wang, W., Smith, D. K., Moulding, K., and Chen, H. M. (1998) The dependence of membrane permeability by the antibacterial peptide cecropin B and its analogs, CB-1 and CB-3, on liposomes of different composition, *J. Biol. Chem. 273*, 27438−27448.
18. Bryson, E. A., Rankin, S. E., Carey, M., Watts, A., and Pinheiro, T. J. T. (1999) Folding of apocytochrome *c* in lipid micelles: Formation of α-helix precedes membrane insertion, *Biochemistry 38*, 9758−9767.
19. Silvestro, L., and Axelsen, P. H. (2000) Membrane-induced folding of cecropin A, *Biophys. J. 79*, 1465−1477.

20. Maddox, M. W., and Longo, M. L. (2002) A Monte Carlo study of peptide insertion into lipid bilayers: Equilibrium conformations and insertion mechanisms, *Biophys. J. 82*, 244−263.
21. Constantinescu, I., and Lafleur, M. (2004) Influence of the lipid composition on the kinetics of concerted insertion and folding of melittin in bilayers, *Biochim. Biophys. Acta 1676*, 26−37.
22. Im, W., and Brooks, C. L. (2005) Interfacial folding and membrane insertion of designed peptides studied by molecular dynamics simulations, *Proc. Natl. Acad. Sci. U.S.A. 102*, 6771−6776.
23. Tucker, M. J., Tang, J., and Gai, F. (2006) Probing the kinetics of membrane-mediated helix folding, *J. Phys. Chem. B 110*, 8105−8109.
24. Bond, P. J., and Sansom, M. S. P. (2006) Insertion and assembly of membrane proteins via simulation, *J. Am. Chem. Soc. 128*, 2697−2704.
25. Golding, C., Senior, S., Wilson, M. T., and O'Shea, P. (1996) Time resolution of binding and membrane insertion of a mitochondrial signal peptide: Correlation with structural changes and evidence for cooperativity, *Biochemistry 35*, 10931−10937.
26. Nymeyer, H., Woolf, T. B., and Garcia, A. E. (2005) Folding is not required for bilayer insertion: Replica exchange simulations of an α-helical peptide with an explicit lipid bilayer, *Proteins 59*, 783−790.
27. Matsuzaki, K., Yoneyama, S., Murase, O., and Miyajima, K. (1996) Transbilayer transport of ions and lipids coupled with mastoparan X translocation, *Biochemistry 35*, 8450−8456.
28. Arbuzova, A., and Schwarz, G. (1999) Pore-forming action of mastoparan peptides on liposomes: A quantitative analysis, *Biochim. Biophys. Acta 1420*, 139−152.
29. Schwarz, G., and Reiter, R. (2001) Negative cooperativity and aggregation in biphasic binding of mastoparan X peptide to membranes with acidic lipids, *Biophys. Chem. 90*, 269−277.
30. Shai, Y. (2002) Mode of action of membrane active antimicrobial peptides, *Biopolymers 66*, 236−248.
31. Higashijima, T., Wakamatsu, K., Takemitsu, M., Fujino, M., Nakajima, T., and Miyazawa, T. (1983) Conformational change of mastoparan from wasp venom on binding with phospholipid membrane, *FEBS Lett. 152*, 227−230.
32. Todokoro, Y., Fujiwara, T., Yumen, I., Fukushima, K., Kang, S. W., Park, J. S., Kohno, T., Wakamatsu, K., and Akutsu, H. (2006) Structure of tightly membrane-bound mastoparan X, a G-protein-activating peptide, determined by solid-state NMR, *Biophys. J. 91*, 1368−1379.
33. Tucker, M. J., Oyola, R., and Gai, F. (2006) A novel fluorescent probe for protein binding and folding studies: p-Cyano-phenylalanine, *Biopolymers 15*, 571−576.
34. Tucker, M. J., Oyola, R., and Gai, F. (2005) Conformational distribution of a 14-residue peptide in solution: A fluorescence resonance energy transfer study, *J. Phys. Chem. B 109*, 4788−4795.
35. Ghadiri, M. R., and Choi, C. (1990) Secondary structure nucleation in peptides. Transition metal ion stabilized α-helices, *J. Am. Chem. Soc. 112*, 1630−1632.
36. Ruan, F. Q., Chen, Y. Q., and Hopkins, P. B. (1990) Metal ion enhanced helicity in synthetic peptides containing unnatural, metal-ligating residues, *J. Am. Chem. Soc. 112*, 9403−9404.
37. Kohn, W. D., Kay, C. M., Sykes, B. D., and Hodges, R. S. (1998) Metal ion induced folding of a de novo designed coiled-coil peptide, *J. Am. Chem. Soc. 120*, 1124−1132.
38. Wittung-Stafshede, P. (2004) Role of cofactors in folding of the blue-copper protein azurin, *Inorg. Chem. 43*, 7926−7933.
39. Dai, Q. Y., Prorok, M., and Castellino, F. J. (2004) A new mechanism for metal ion-assisted interchain helix assembly in a naturally occurring peptide mediated by optimally spaced γ-carboxyglutamic acid residues, *J. Mol. Biol. 336*, 731−744.
40. Handel, T. M., Williams, S. A., and DeGrado, W. F. (1993) Metal-ion dependent modulation of the dynamics of a designed protein, *Science 261*, 879−885.
41. Krantz, B. A., and Sosnick, T. R. (2001) Engineered metal binding sites map the heterogeneous folding landscape of a coiled coil, *Nat. Struct. Biol. 8*, 1042−1047.
42. Krantz, B. A., Dothager, R. S., and Sosnick, T. R. (2004) Discerning the structure and energy of multiple transition states in protein folding using ψ-analysis, *J. Mol. Biol. 337*, 463−475.
43. Pandit, A. D., Jha, A., Freed, K. F., and Sosnick, T. R. (2006) Small proteins fold through transition states with native-like topologies, *J. Mol. Biol. 361*, 755−770.
44. Signarvic, R. S. (2006) The de novo design of molecular switches: Manipulation of secondary structure to modulate conformational stability, Ph.D. Dissertation, University of Pennsylvania, Philadelphia, PA.
45. Hutnik, C. M., and Szabo, A. G. (1989) A time-resolved fluorescence study of azurin and metallozaurin derivatives, *Biochemistry 28*, 3935−3939.
46. De Pina, K., Navarro, C., McWalter, L., Boxer, D. H., Price, N. C., Kelly, S. M., Mandrand-Berthelot, M. A., and Wu, L. F. (1995) Purification and characterization of the periplasmic nickel-binding protein NikA of *Escherichia coli* K12, *Eur. J. Biochem. 227*, 857−865.
47. Papo, N., and Shai, Y. (2003) Exploring peptide membrane interaction using surface plasmon resonance: Differentiation between pore formation versus membrane disruption by lytic peptides, *Biochemistry 42*, 458−466.
48. Whiles, J. A., Brasseur, R., Glover, K. J., Melacini, G., Komives, E. A., and Vold, R. R. (2001) Orientation and effects of mastoparan X on phospholipid bicelles, *Biophys. J. 80*, 280−293.
49. Arbuzova, A., Murray, D., and McLaughlin, S. (1998) MARCKS, membranes, and calmodulin: Kinetics of their interaction, *Biochim. Biophys. Acta 1376*, 369−379.
50. Pokorny, A., Birkbeck, T. H., and Almeida, P. F. F. (2002) Mechanism and kinetics of δ-lysin interaction with phospholipid vesicles, *Biochemistry 41*, 11044−11056.
51. Cline, D. J., Thorpe, C., and Schneider, J. P. (2003) Effects of As(III) binding on α-helical structure, *J. Am. Chem. Soc. 125*, 2923−2929.
52. Matsuzaki, K. (1999) Why and how are peptide-lipid interactions utilized for self-defense? Magainins and tachyplesins as archetypes, *Biochim. Biophys. Acta 1462*, 1−10.
53. Wang, T., Lau, W. L., DeGrado, W. F., and Gai, F. (2005) *T*-jump infrared study of the folding mechanism of coiled-coil GCN4-p1, *Biophys. J. 89*, 4180−4187.
54. Wang, T., Zhou, Z., Bunagan, M. R., Du, D., Bai, Y., and Gai, F. (2007) Probing the folding intermediate of Rd-apocyt b562 by protein engineering and infrared *T*-jump, *Protein Sci. 16*, 1176−1183.
55. Wang, T., Du, D. G., and Gai, F. (2003) Helix-coil kinetics of two 14-residue peptides, *Chem. Phys. Lett. 370*, 842−848.
56. Du, D. G., Bunagan, M. R., and Gai, F. (2007) The effect of charge-charge interactions on the kinetics of α-helix formation, *Biophys. J.* (doi: 10.1529/biophysj.107.108498).
57. Shai, Y., and Oren, Z. (2001) From "carpet" mechanism to de-novo designed diastereomeric cell-selective antimicrobial peptides, *Peptides 22*, 1629−1641.
58. Schmitt, M. A., Weisblum, B., and Gellman, S. H. (2007) Interplay among folding, sequence, and lipophilicity in the antibacterial and hemolytic activities of α/β-peptides, *J. Am. Chem. Soc. 129*, 417−428.
59. Kuroda, K., and DeGrado, W. F. (2005) Amphiphilic polymethacrylate derivatives as antimicrobial agents, *J. Am. Chem. Soc. 127*, 4128−4129.
60. Ivanov, I., Vemparala, S., Pophristic, V., Kuroda, K., DeGrado, W. F., McCammon, J. A., and Klein, M. L. (2006) Characterization of nonbiological antimicrobial polymers in aqueous solution and at water-lipid interfaces from all-atom molecular dynamics, *J. Am. Chem. Soc. 128*, 1778−1779.
61. McLaughlin, A., Grathwoh, C., and McLaughlin, S. (1978) The adsorption of divalent cations to phosphatidylcholine bilayer membranes, *Biochim. Biophys. Acta 513*, 338−357.
62. Vest, R. S., Gonzales, L. J., Permann, S. A., Spencer, E., Hansen, L. D., Judd, A. M., and Bell, J. D. (2004) Divalent cations increase lipid order in erythrocytes and susceptibility to secretory phospholipase $A_2$, *Biophys. J. 86*, 2251−2260.


BI7018404